Research Article | Vol. 30, No. 5 / 28 Feb 2022 / Optics Express 7210
Optics EXPRESS

Numerical methods for generation and characterization of disordered aperiodic photonic lattices

DEJAN V. TIMOTIJEVIĆ,[1] JADRANKA M. VASILJEVIĆ,[2,*] AND DRAGANA M. JOVIĆ SAVIĆ[2]

[1] *Institute for Multidisciplinary Research, University of Belgrade, Kneza Višeslava 1, 11030, Belgrade, Serbia*
[2] *Institute of Physics, University of Belgrade, P.O. Box 68, 11001 Belgrade, Serbia*
[*] *jadranka@ipb.ac.rs*

Abstract: We introduce numerical modeling of two different methods for the deterministic randomization of two-dimensional aperiodic photonic lattices based on Mathieu beams, optically induced in a photorefractive media. For both methods we compare light transport and localization in such lattices along the propagation, for various disorder strengths. A disorder-enhanced light transport is observed for all disorder strengths. With increasing disorder strength light transport becomes diffusive-like and with further increase of disorder strength the Anderson localization is observed. This trend is more noticeable for longer propagation distances. The influence of input lattice intensity on the localization effects is studied. The difference in light transport between two randomization methods is attributed to various levels of input lattice intensity. We observe more pronounced localization for one of the methods. Localization lengths differ along different directions, due to the crystal and lattice anisotropy. We analyze localization effects comparing uniform and on-site probe beam excitation positions and different probe beam widths.

1. Introduction

The phenomenon of Anderson localization (AL) originally discovered a few decades ago is one of the basic prominent phenomena in solid-state physics [1,2]. Originally introduced to explain the localization of electronic wave functions in disordered crystals, it has found growing applications in a variety of classical and quantum systems [3–5], including light waves in different materials [6–8]. AL of light has achieved renewed interest due to the potential for the realization of localization of optical waves in random media, especially in discrete systems [9], laser-written waveguide arrays [10–13], and/or optically induced randomized potential [14]. It is in the focus of investigations, especially in nonlinear optics and photonics, due to the development of new optical technologies and media, such as disordered photonic crystals and photonic lattices, in which the presence of AL appreciably changes the propagation of light [15–17]. Owing to the analogy of paraxial photonic systems to solid-state systems, where the wave function evolution corresponds to propagation of light and thanks to the fact that longitudinally invariant disorder can be effectively realized in lattices, experimental activities in AL of light started to attract the attention of optical community [8].

Up to now, periodic photonic structures have led to light control by photonic band gaps in space and time, whereas random photonic structures give rise to localization [6,8,18]. Dynamical control and manipulation of light by deterministic aperiodic or complex photonic structures [19–21] at the intersection between periodic and random crystal structures, especially the randomization of aperiodic structures, have not yet been fully understood nor exploited for applications. Two-dimensional aperiodic photonic lattices were experimentally realized by the optical induction technique in photorefractive crystal by different combinations of nondiffracting

#447572 https://doi.org/10.1364/OE.447572
Journal © 2022 Received 7 Nov 2021; revised 20 Jan 2022; accepted 2 Feb 2022; published 17 Feb 2022

Optics EXPRESS

Mathieu beams [22], combining them in metastructures by splicing in both transverse dimensions with different offsets, thus allowing for the tunable optical response. Nondiffracting beams are convenient for the generation of photonic lattices by optical induction technique since they have propagation invariant property that is retained under the condition of week nonlinearity [23]. There are four nondiffracting beam families that are exact solutions of the Helmholtz equation in different coordinate systems [24,25]: plane waves in Cartesian, Bessel beams in circular cylindrical [26], Mathieu beams in elliptic cylindrical [27], and parabolic beams in parabolic cylindrical coordinates [28].

Aperiodic lattices in contrast to periodic lattices contain non-uniform distances between the lattice sites with non-homogeneous intensity depths distributions, therefore light propagation strongly depends on the probe beam excitation position local environments [29–31]. Such lattices including quasiperiodic Penrose and Fibonacci, and aperiodic Mathieu lattice, are shown to hamper diffraction of linear light [30,31] which can be explained by excitation of highly localized linear modes [32]. Such lattices also support nonlinear light localization [29,31]. Disordering periodic lattices can lead to AL [7,8] or its suppression [33], referred therein as inverse Anderson transition. AL is enhanced by self-focusing nonlinearity in disordered periodic lattice [7,8]. Disordered quasiperiodic Penrose lattice can support AL and disorder-enhanced transport (DET) which is associated with broadening of eigenfunctions with the disorder. Instead of a singular pattern of quasiperiodic structures such as Penrose or Fibonacci with limited variation in probing local environments, we are proposing consideration of a whole class of aperiodic structures based on Mathieu beams [22] with the adjustable spatial and intensity distribution, thus providing different probing local environments, as well as introducing structure anisotropy variability. A further step is randomization of such class of aperiodic structures in order to create an appropriate platform for investigation of light propagation effects and study their possible transition to AL or DET, which is still an unexplored topic. Exhaustive theoretical or experimental analysis of light propagation in such a large class of aperiodic structures is difficult to implement, therefore, in this paper, we focused on one exemplary aperiodic Mathieu structure and numerically model their possible randomizations and probing of resulting disordered lattices.

In this article, we introduce the modeling of two different methods for the generation of two-dimensional propagation invariant disordered aperiodic Mathieu lattices, corresponding to two different experimental realizations using optical induction technique in a photorefractive crystal. One of the methods corresponds to the already known randomization method [32] with potentially simpler experimental realization such as we use in our previous studies. But for the first time, we suggest a substantially different randomization method and compare them with the previous method, with additional improvement. We present a comprehensive numerical study of transverse light localization in such waveguides arrays. We aim at elucidating the effect of disorder on light propagation considering localization effects along propagation. The influence of lattice intensity on the diffraction rate is also analyzed; specifically differences in the localization while varying a nominal lattice intensity, as well as investigating the averaged lattice intensity. We discuss the effect of different choices for input excitation sites on the disorder-induced localization in such a system. Finally, the effect of the probe beam width on the localization effects is studied.

By gradually adding disorder to the lattice we demonstrate enhanced light transport of the probe beams for all disorder strengths, as well as show the transition from diffusive-like transport to the AL for higher disorder levels. More pronounced localization is observed for longer propagation distances even for lower disorder levels. We attribute effective beam width difference between two randomization methods to varying levels of lattice intensities. We observe more pronounced localization for one of the methods; shorter localization length decreases indicating more pronounced localization. It is shown that localization length differs along different directions, which we attribute to the lattice and crystal anisotropy. There is no noticeable difference in

Optics EXPRESS

localization effects when probe beam excitation positions are distributed only on-site instead of uniformly. For broad Gaussian probe beams localization is not observed in such lattices.

2. Numerical modeling of light propagation in disordered lattices

By solving the coupled nonlocal system of two equations: the nonlinear Schrödinger equation, as propagation equation and a potential equation [34], we numerically simulate the weak nonlinear propagation of probe beam in the photorefractive cerium-doped strontium barium niobate (SBN) crystal with disordered aperiodic Mathieu lattices modeled as propagation invariant potential. Both propagation and potential equations are initial values problems with absorbing boundaries numerically solved by the symmetrized spectral split-step beam propagation method [35]. The propagation equation for an initial extraordinary polarized scalar electric field A (probe beam) with longitudinal wave vector k_z is

$$\mathrm{i}\partial_z A + \frac{1}{2k_z}\Delta_\perp A + \frac{k_z}{2n_{\mathrm{o,e}}^2}\delta n^2\left(|A|^2\right)A = 0. \tag{1}$$

The wave number $k = 2\pi/\lambda = \sqrt{\left(k_\perp^2 + k_z^2\right)}$ is defined by the wavelength $\lambda = 532\,\mathrm{nm}$. The potential in this equation is given by nonlinear refractive index $\delta n^2\left(|A|^2\right) = -n_{\mathrm{o,e}}^4 r_{13,33}E$, where $n_\mathrm{e} = 2.325$ and $n_\mathrm{o} = 2.358$ are the extraordinary and ordinary indices, and $r_{13} = 47\,\mathrm{pm/V}$, $r_{33} = 237\,\mathrm{pm/V}$ are corresponding electro-optic coefficients of photorefractive birefringent SBN crystal, respectively. The electric field $E = E_\mathrm{ext} + E_\mathrm{sc}$ that builds up inside the SBN crystal is a superposition of an external electric field $E_\mathrm{ext} = 2000\,\mathrm{V/cm}$ and an internal space charge field E_sc that is determined by the intensity distribution $I = |A|^2$ with a potential equation. The external electric field E_ext is aligned with the optical $c = x$-axis, perpendicular to the $z-$ axis, the direction of propagation, that is parallel to the long axis of the crystal.

In order to take photorefractive material response as well as the electric bias of the SBN crystal into account, we deploy the anisotropic, diffusive potential equation for the spatial evolution of the electrostatic potential ϕ_{sc} of the optically induced space-charge field E_sc,

$$\Delta_\perp\phi_\mathrm{sc} + \nabla_\perp \ln\left(1 + I + I_{DL}\right)\cdot\nabla_\perp\phi_\mathrm{sc} = E_\mathrm{ext}\partial_x \ln\left(1 + I + I_{DL}\right), \tag{2}$$

where I is obtained from Eq. (1) and subsequently Eq. (1) is updated with $E_\mathrm{sc} = \partial_x\phi_{sc}$, iteratively. Disordered lattice intensity distribution $I_{DL} = |A_{DL}|^2$, with input lattice intensity I_in, modeling transverse intensity distribution of nondiffracting pattern homogeneous in the propagation direction, is persistent through iterations. Experimental laser power P is connected with I_{DL} via I_in. Intensity and spatial distribution of I_{DL} determine $\delta n^2\left(|A|^2\right)$ in Eq. (1) through iterations. In this way, instead of modeling refractive index modulation $\delta n^2\left(|A|^2\right)$ directly, we model its underlying cause. Potential $I_{DL} = |A_{DL}|^2$ of disordered lattices ***DL*** is formed by coherently adding the two-dimensional original structure ***L*** and disorder pattern ***D*** with same maximum structure intensity according to the relation

$$A_{DL} = (1 - p) * A_L + p * A_D, \tag{3}$$

where A stands for field amplitude. Parameter p is the relative contribution of the original structure and disorder pattern, which we identify as disorder strength (disorder level). By varying p ($0 \le p \le 1$), considering it a uniform measure of disorder strength, we gradually adjust the level of lattice disorder relative to the original, undisturbed structure.

The whole process of writing propagation invariant disordered lattice is here abstracted and modeled through potential I_{DL} in Eq. (2), which we will further refer as a writing lattice pattern.

Optics EXPRESS

Justification of substitution of the writing process with model potential I_{DL} is based on numerically simulation of writing process and the experimental realization of propagation invariant photonic lattices in SBN crystal as in our previous publication [22]. The same writing simulation is carried out as part of our preparation procedure to find a range of input lattice intensities I_{in} for which aperiodic Mathieu lattice stays stable and propagation invariant through the SBN crystal.

3. Two methods for the generation of disordered lattices

Here, we present two methods for the realization of two-dimensional propagation invariant disordered photonic lattices with adjustable disorder strength. We calculated the complex light field of disordered lattice for any disorder strength according to Eq. (3). Such calculated complex light fields of disordered lattices can be used as the writing light patterns for the generation of waveguide lattice by optical induction in the SBN crystal. Previous studies that applied the optical induction technique for realization of photonic lattices in birefringent SBN crystal, externally biased with an electric field aligned along the optical $c = x$-axis, and perpendicular to the propagation direction (z-axis), used the ordinary polarized writing beam with a laser power P, considered to be fairly linear in SBN crystal.

For each disorder strength, when the maximum lattice intensity of the resulting disordered lattice is left unscaled, we will refer to that case as the first method (*M1*), and laser power for experimental realization will vary with change disorder strength. The second method (*M2*) is characterized with scaling I_{DL} with I_{in} for each disorder strength, which effectively keeps the experimental lesser power constant. This distinction in methods results is the result of differences in potential experimental realizations.

For the proposed fabrication of the disordered lattices by the optical induction technique, which corresponds to M1 and M2 we can use our experimental setup from our previous study [22] using one spatial light modulator (SLM) which modulated writing beam, producing computer generating hologram. Another way for experimental realization of M1 based on experimental setup presented in Ref. [32] is to split the structure beam into two parts with controllable powers. The complex light field of the original structure would modify one part of the structure beam by the first SLM, while the complex light field of the disorder pattern addressed on the second SLM would modify the other part of the structure beam. Afterward, those two structure beams, which spectra in the transverse Fourier space are set to be located on the same circle with radius k to ensure the same propagation constant, coherently interfere to create propagation invariant disordered aperiodic lattice. In this way, a relative disorder strength would be indirectly deduced from structure beam powers.

In this paper, as the original undisturbed structure $\boldsymbol{L}$, we use aperiodic Mathieu structure designed by Mathieu Gauss beams, introduced in our previously paper [22]. Disorder pattern $\boldsymbol{D}$ is numerically calculated by interfering plane waves with constant amplitude and random phases, to generate the propagation invariant structure with random pattern in transverse dimension. We generate the disorder pattern whose spectrum in the transverse Fourier space is located on the same circle with radius k as the original undisturbed structure [36], to crate propagation invariant structures with the same propagation constant. The disorder pattern's mean grain size $2\pi/k$ is equal to the characteristic structure size $a = 25\mu m$ of Mathieu Gauss beams, used for the realization of the aperiodic structure. Transverse intensity distributions of the original aperiodic Mathieu structure and disorder pattern, that constitute disordered lattice $\boldsymbol{DL}$ created according to Eq. (3), are shown in Figs. 1 (A1) and (B1), respectively. By increasing disorder strength we change the geometry of the original structure until we completely substitute the original structure with a disorder pattern. As the difference in methods causes two choices of intensity scaling, we will investigate and compare the consequences of such scaling options. For both methods, variation of disorder strength p leads to the variation of writing lattice intensity, effectively correlating disorder strength with writing lattice intensity and indirectly with optically induced

Optics EXPRESS

refractive index modulation inside the crystal. For the same disorder levels averaged lattice intensities differ for M1 and M2, causing differentiation in propagation characteristics under these method's conditions. Transverse intensity distributions of disordered aperiodic lattices with 40% disorder for these two methods are presented in Fig. 1 (C1) and Fig. 1 (D1). Their displayed area is less than 3% of the whole transversal computational space.

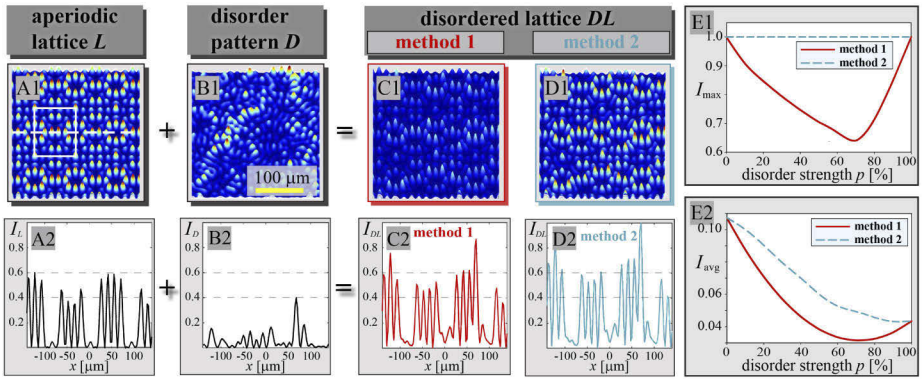

Fig. 1. Two methods of modeling disordered lattices. The transverse intensity distribution of: (A1) aperiodic lattice, with white box indicating typical pattern; (B1) disorder pattern; (C1) and (D1) disordered aperiodic lattices with 40% disorder for M1 and M2, respectively. (A2) - (D2) Corresponding representative lattice intensity cross-section taken along the x-axis marked with a white dashed line in (A1); dashed lines indicate maximum intensities of original lattice and disorder pattern. The maximum lattice intensity (E1) and the averaged lattice intensities (E2) versus disorder strength for different methods.

As an illustration of Eq. (3) in Figs. 1 (A2) - (D2) we present a single typical intensity cross-section along the x-axis (y-position indicated with a dashed line in Fig. 1 (A1)) for aperiodic lattice, disorder pattern, and resulting disordered aperiodic lattices with 40% disorder for two different methods. Levels for $p = 0.4$ and $1 - p = 0.6$ are dashed and coincide with maximum intensities of disorder and aperiodic structure, respectively. Unlike the periodic lattice, our aperiodic lattice is not uniform in the waveguide's distances and their depths vary. For M1 and M2 spatial distribution of the disordered aperiodic lattices are the same, but they differ in waveguides depths as M2 intensity values are greater than M1 intensity values (red and blue plots in Figs. 1 (C2) and (D2)).

We noted that the disorder strength p changes the lattice intensity, hence in addition to maximum lattice intensity $I_{\max}$, we calculate averaged lattice intensity $I_{\text{avg}} = \sum_r I_{DL}(\mathbf{r}) = \sum_{\mathbf{r}} |A_{DL}(\mathbf{r})|^2$, representing the level of influence of potential term in Eq. (2). The resulting differentiation of our methods in $I_{\max}$ and I_{avg} dependence on disorder strength is shown in Figs. 1 (E1) and (E2), respectively. In the first method disordered aperiodic maximum lattice intensity and the averaged lattice intensity decrease from 0% to 70% disorder, afterward increase. For 100% disorder, only maximum lattice intensity returns to an input value. In the second method, the maximum lattice intensity of disordered aperiodic lattice is equal to I_{in} for all disorder strengths, but averaged lattice intensity always decreases with increasing disorder strength. Both the maximum lattice intensity and the averaged lattice intensity for M1 are lower than for M2, except for 0% and 100% disorder. Assuming the same disorder pattern, both methods produce the same lattices for 0% and 100% disorder strengths we will exclude these two endpoints when we discuss method differences.

Optics EXPRESS

4. Quantitative description of localization phenomenon

To investigate the transverse light localization in disordered lattices, we statistically analyzed probe beam propagation for different excitation positions selected to involve various local environments. For probe beam excitation positions we use an equidistant 8×8 grid covering one complete typical pattern depicted in Fig. 1 (A1). We performed such analysis, averaging 64 various probe beam intensity distributions at the different propagation distances, for several disorder levels. For each disorder level, we have different realizations of the disordered lattice that are spatially similar due to fixed deterministic disorder pattern with statistical sampling spanning excitation probe positions only (N=64). In the preliminary investigations, we perform statistics with several different fixed disorder patterns and concluded that the statistical quantities and their dependence of disorder we want to report are not significantly influenced by the choice of disorder pattern. Due to the aperiodicity of our lattice, not each typical pattern is the same so we perform N=64 statistics on several of them, again finding no significant variation in statistical quantities of interest. Based on this preliminary analysis we did not vary the disorder pattern between different realizations of disordered lattices.

For comparison, in addition to sampling equidistant excitation positions (uniform), we also perform the statistical analysis sampling on-site positions, exciting only positions of waveguides. On-site excitation positions are chosen according to the positions of aperiodic lattice waveguides, which implies that for higher disorder strengths these positions become less accurate as waveguide's positions and depths are modified by randomization. The process of defining and numerically detecting waveguides positions modified by disorder is time-consuming and we did not pursue it, therefore we abstained from giving strong conclusions regarding on-site positioning at higher disorder levels.

In order to characterize light propagation and localization, we calculate the effective beam width along the propagation distance z according to the relation

$$W_{eff}(z) = P(z)^{-1/2}, \tag{4}$$

where $\mathrm{P}(z) = (\int |A(x,y,z)|^4 dxdy)/(\int |A(x,y,z)|^2 dxdy)^2$ is the inverse participation ratio [8]. We present scaled averaged effective beam width $\langle \omega_{\mathrm{eff}} \rangle = W_{\mathrm{eff}}(z)/(W_{\mathrm{eff}}(0)/FWHM)$ where $FWHM$ is probe beam full width at half maximum. In addition to averaged transverse output intensity distribution, we consider the log-plot profiles of such output intensity distributions to further describe light propagation. Parabolic log-plot fit indicates diffusive-like transport. The exponential decay of the transverse intensity distribution profile determines light localization, hence the linear fit of log-plots of such intensity profiles around the center demonstrates AL. In the region of disorder strength where AL occurs, we obtain localization length ξ_x along the x-axis by fitting intensity profiles $\mathrm{I}(x, y_0)$ with the exponential function

$$I(x, y_0) = \exp\left(-2\frac{|x - x_0|}{\xi_x}\right), \tag{5}$$

where x_0, y_0 denote the position of the beam center. The analogous procedure is applied along the y-direction. In some intermediate cases, when the linear fit is not obvious we compare the goodness of fit of parabolic and linear fits, where higher goodness of fit (closer to 1) indicates preferable fitting of the log plots. Hence, we use the goodness of fit to confirm a suitable fit, linear, or parabolic i.e. to discern the diffusive-like transport or AL. By shrinking the domain where we fit log-plots we notice an increase of the goodness of fit, indicating that localization occurs in a finite central domain, not in whole computation space.

5. Light transport and localization in disordered aperiodic lattices

We compare effects along light propagation in disordered aperiodic lattices generated with two different randomization methods. Figure 2 summarizes the difference between the two methods

Optics EXPRESS

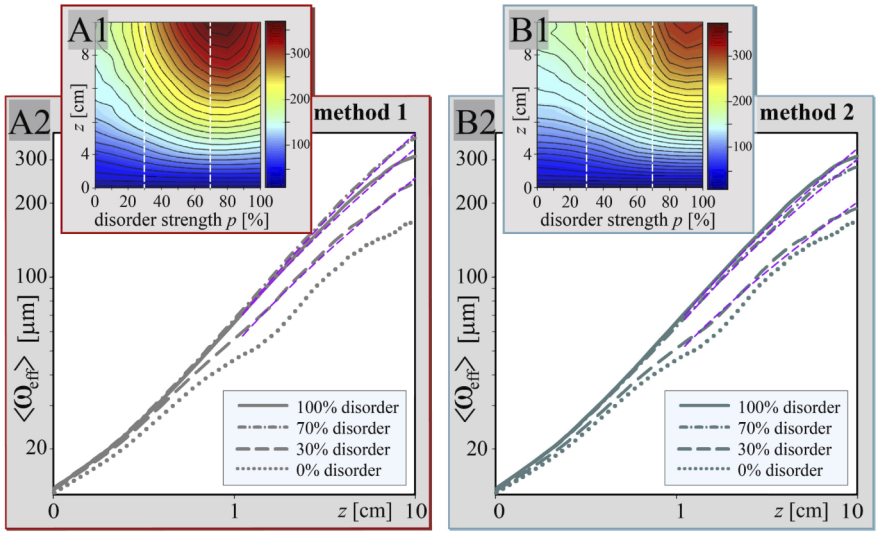

Fig. 2. Comparison of diffraction dependence on disorder strength and propagation distance for two methods. $\langle\omega_{\text{eff}}\rangle$ for various disorder strengths along the propagation distance for: (A1) M1, and (B1) M2; the colormaps display $\langle\omega_{\text{eff}}\rangle$ [μm]. $\langle\omega_{\text{eff}}\rangle$ along the propagation distance for 0%, 30%, 70%, 100% disorder strengths on a double logarithmic scale for: (A2) M1, and (B2) M2. Parameters: input Gaussian probe beam *FWHM* is 8 μm and $I_{\text{in}} = 0.7$.

considering scaled averaged effective beam width $\langle\omega_{\text{eff}}\rangle$. Figures 2 (A1), (B1) display the difference between the two methods presenting $\langle\omega_{\text{eff}}\rangle$ along the propagation distance for various disorder strengths. $\langle\omega_{\text{eff}}\rangle$ during the propagation increases for all disorder strengths. Beam expansion is maximal in the region of 60% to 80% disorder strength for M1 (Fig. 2 (A1)), and in the region of 80% to 90% disorder strength for M2 (Fig. 2 (B1)) indicated with a distribution of points where black isolines cross vertical sections. Examining the horizontal cross-sections from Figs. 2 (A1) and (B1) for each propagation length we confirm DET occurrence. For both methods during the propagation when disorder strengths deviate from that region, we observe the deceleration of $\langle\omega_{\text{eff}}\rangle$ increase. For deviation from disorder strength with maximal beam expansion toward lower disorder strengths, we observe a reduction of DET while for deviation toward higher disorder strengths reduction of DET could be attributed to AL. But, in the case of our lattice, this process is strongly mediated with variation in aggregate lattice intensity, so that we could not identify AL as the sole cause. To confirm that AL of light occurs, and for which disorder levels, we will investigate where the log-plots of the averaged intensity distributions are linearly fitted near the center.

For both methods, in Figs. 2 (A2), (B2) we present $\langle\omega_{\text{eff}}\rangle$ as a function of propagation distance z (on a double logarithmic scale), for four disorder strengths. A purple dashed lines define fits of $\langle\omega_{\text{eff}}\rangle$ by power-law $\langle\omega_{\text{eff}}\rangle(z) \propto z^{\nu}$, for M1 and M2, respectively. ν corresponds to beam expansion rate: $\nu = 1$ signifying ballistic transport and $\nu = 0.5$ characterize diffusive-like transport. For a short propagation distance (z<1 cm), beam expansion is almost linear ($\nu = 1$ i.e. ballistic transport). For a longer propagation distance (from 1 cm to 10 cm), the beam expansion rate is closest to $\nu = 0.5$ i.e. diffusive-like transport. For M1 is maximal for 70% $\nu = 0.52$ and lower $\nu = 0.48$ for both 30% and 100%. For M2 the beam expansion rate is maximal for 100% $\nu = 0.48$ and lower for 70% and 30%, $\nu = 0.47$ and $\nu = 0.45$, respectively.

For both methods in the disordered aperiodic lattice with any percent of disorder $\langle\omega_{\text{eff}}\rangle$ is greater than in the lattice without disorder indicating DET, which could be explained that disorder spreads linear modes [32] (Fig. 3 (A)). At the shorter propagation distance ($z = 2$ cm), $\langle\omega_{\text{eff}}\rangle$s

Optics EXPRESS

are increasing with increasing disorder strength. A broadening of the beam is more pronounced for longer propagation distances (z = 6 cm and 10 cm). There we notice that $\langle\omega_{\text{eff}}\rangle$s at the fixed propagation distances are increasing up to the maximum values which occur at disorder strength 80% for M1 and 90% for M2, indicating maximum of DET. With the further increase of disorder strength, $\langle\omega_{\text{eff}}\rangle$s are decreasing indicating the possibility of AL occurrence. Corresponding $\langle\omega_{\text{eff}}\rangle$s have greater values for M1 than for M2, which is easily discerned from Fig. 3 (A).

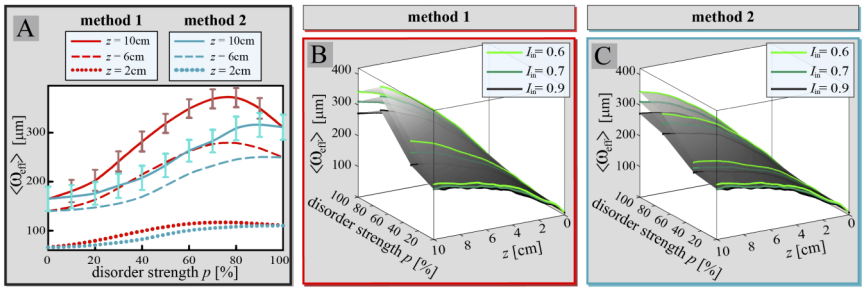

Fig. 3. Influence of disorder strength p and input lattice intensity I_{in} on the light diffraction. (A) $\langle\omega_{\text{eff}}\rangle$ versus disorder strength after 2 cm, 6 cm, and 10 cm of propagation for $I_{\text{in}} = 0.7$ for both methods. The error bars are the statistical standard deviations of $\langle\omega_{\text{eff}}\rangle$. (B) M1 and (C) M2: interpolated surfaces of $\langle\omega_{\text{eff}}\rangle$ along the propagation distance for 0%, 30%, 70%, 100% disorder strengths and for various I_{in}. Other parameters are as in Fig. 2.

The following study is the independent verification of the influence of input lattice intensity I_{in} on diffraction. We compare $\langle\omega_{\text{eff}}\rangle$s in dependence of disorder strength along propagation distance for 3 different values of the input lattice intensity I_{in}. Figures 3 (B), (C) summarize $\langle\omega_{\text{eff}}\rangle$ for two methods where we highlight lines of constant disorder strength along the propagation distance. By observing slopes of highlighted lines for each I_{in}, we illustrate the beam expansion explained in the description of Fig. 2. For all disorder strengths and propagation distances, we observe the direct influence of lattice intensity on diffraction, for both methods, where lowering I_{in} causes an increase in $\langle\omega_{\text{eff}}\rangle$. Since the explicit independent increase in lattice intensity leads to a similar effect as the inclusion of weak nonlinearity in disordered lattices, indirect change in intensity due to correlation with variation of disorder strength can also influence AL [7,8]. This effect will especially be visible in Figs. 6 and 7, where comparing log-plots of average intensity distributions for two methods for the same higher disorder strengths, observing that M1 which has lower lattice intensity than M2, produces lover central picks and higher tails, similar to Refs. [7,8].

The main difference in our methods is caused by the difference in the maximum lattice intensity I_{max}, which is varying with change of disorder strength for the first method, while it is constant for the second method, as well as different variations of the averaged lattice intensities I_{avg} with the change of disorder strength for different methods (Figs. 1 (E1), (E2)). For both methods, $\langle\omega_{\text{eff}}\rangle$ variation versus disorder strength is different for different propagation distances (Fig. 3 (A)). We notice that $\langle\omega_{\text{eff}}\rangle$s after a longer propagation distance (10 cm), have a dependence on disorder strength similar to I_{avg} (Fig. 1 (E2)). Hence, to investigate this connection, we normalize $\langle\omega_{\text{eff}}\rangle$ and reciprocal averaged lattice intensity $(I_{\text{avg}})^{-1}$ according to relation $F(p)/(F(1) - F(0)) - F(0)$, where F is $\langle\omega_{\text{eff}}\rangle$ or $(I_{\text{avg}})^{-1}$, and p is disorder strength. We present them, as well as their differences in Fig. 4 for both methods. For both methods, variations of normalized $\langle\omega_{\text{eff}}\rangle$ closely follow $(I_{\text{avg}})^{-1}$. Therefore, we conclude that $\langle\omega_{\text{eff}}\rangle$ is strongly influenced with the variation in $(I_{\text{avg}})^{-1}$ versus disorder strength for longer propagation distances, for narrow probe beam width.

Deviation of $\langle\omega_{\text{eff}}\rangle$ and $(I_{\text{avg}})^{-1}$ graphs is quantified with their difference, quantity that contains the influence of parameters not directly connected to the lattice intensity, such as lattice and beam shapes. For M2 where the dependence of $(I_{\text{avg}})^{-1}$ on p is monotonous, distributions of $\langle\omega_{\text{eff}}\rangle$ and

Optics EXPRESS

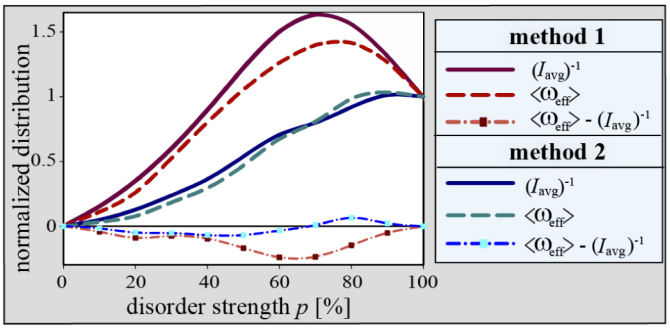

Fig. 4. Comparison of methods via $\langle\omega_{\text{eff}}\rangle$ and $(I_{\text{avg}})^{-1}$. Normalized $\langle\omega_{\text{eff}}\rangle$, $(I_{\text{avg}})^{-1}$ and their differences for both methods as a function of disorder strength. Other parameters are as in Fig. 2.

$(I_{\text{avg}})^{-1}$ and $(I_{\text{avg}})^{-1}$ vs. p closely overlap. We associate a dip of deviation for M1 in Fig. 4 with a sharp minimum in dependence of the maximum lattice intensity I_{max} versus p (Fig. 1 (E1)) and also with a minimum in I_{avg} versus p (Fig. 1 (E2)), occurring at the same disorder level. As we demonstrate in Fig. 3, light diffraction is reverse proportional to input lattice intensity. Hence, for the minimum of the maximum lattice intensity in M1, we have the highest $\langle\omega_{\text{eff}}\rangle$ (maximal DET). The narrow probe beam for low lattice intensity diffracts the most, but at longer propagation distances $\langle\omega_{\text{eff}}\rangle$ does not reach the variation of I_{avg} as at minimal lattice intensities beam already rapidly expanded early in propagation. Further in this section, we will independently study probe beam width influence on diffraction in our lattice.

We analyze the averaged transverse intensity distributions of probe beam along the propagation distance by using the log-plot cross sections of averaged intensity distributions and localization lengths. Figures 5 (A) - (D) summarize the averaged transverse intensity distributions of probe beam for some disorder strengths and some propagation distances. Parallelly, we investigate a suitable log-plot cross section along the x-axis (gray/red/cyan plots) and y-axis (black/dark red/dark cyan plots) in Fig. 6.

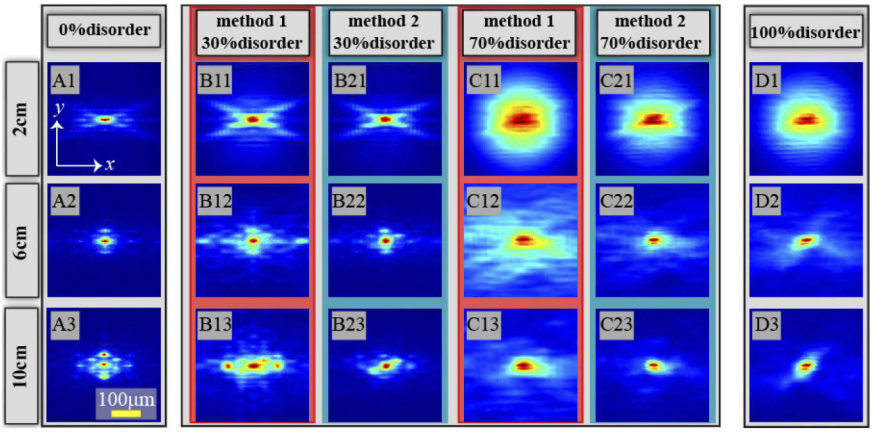

Fig. 5. Disorder-induced light transport and localization in aperiodic Mathieu lattice. Numerically averaged intensity distributions at the lattice output for different disorder strengths at different propagation distances. Other parameters are as in Fig. 2.

Optics EXPRESS

Figure 5 (A) depicts averaged intensity distribution in aperiodic lattice without the disorder, for 3 different propagation distances (2 cm, 6 cm, and 10 cm), demonstrating discrete diffraction of light, also visible in Fig. 6 (A). Figures 5 (B), (C) present averaged intensity distributions for two values of disorder strength (30% and 70%) after 3 propagation distances for both methods; suitable log-plot cross section along the x-axis (red and cyan plots) and y-axis (dark red and dark cyan plots) are presented in Figs. 6 (B), (C). For 30% disorder averaged intensity distributions and the log-plot cross sections near the center are broader for M1 than for M2. More pronounced diffraction, i.e. DET for M1 is evident (Figs. 5 (B), Fig. 6 (B)). Also, the less pronounced diffraction of light along the y-direction, for both methods, is noticeable due to the crystal ($r_{33}>>r_{13}$) and lattice anisotropy (Fig. 1 (A1)).

With further increasing disorder strength (>30%), averaged intensity distributions and the log-plot cross sections near the center are broadened, indicating DET. Additionally, the diffraction and localization effects are more noticeable along the y-transverse direction, for both methods, due to the crystal and lattice anisotropy: as visible for 70% disorder strength at $z = 2$ cm (Figs. 6 (C11), and (C21)). The interplay of lattice and crystal anisotropy influence is evident for shorter propagation distances in the log-plot cross sections near the center for M1 (Figs. 6 (C11)), where the log-plot along the x-axis is fitted with parabola, indicating diffusive-like transport, while the log-plot along the y-axis is linearly fitted indicating light localization. At the same time, as the influence of lattice anisotropy is mediated with lattice intensity, for M2 the log-plots cross sections near the center along the x- and y-axis are linearly fitted (Fig. 6 (C21)). The localization length is shorter along the y-axis, indicating that localization is still stronger in this direction. The influence of the lattice and crystal anisotropy persists for longer propagation distances (Figs. 6 (C12), (C22), (C13), (C23)), which will be illustrated with different localization lengths along the x- and y-direction in Fig. 8. Also, localization lengths in both directions for M2 are shorter than for M1, which shows that stronger localization occurs for M2.

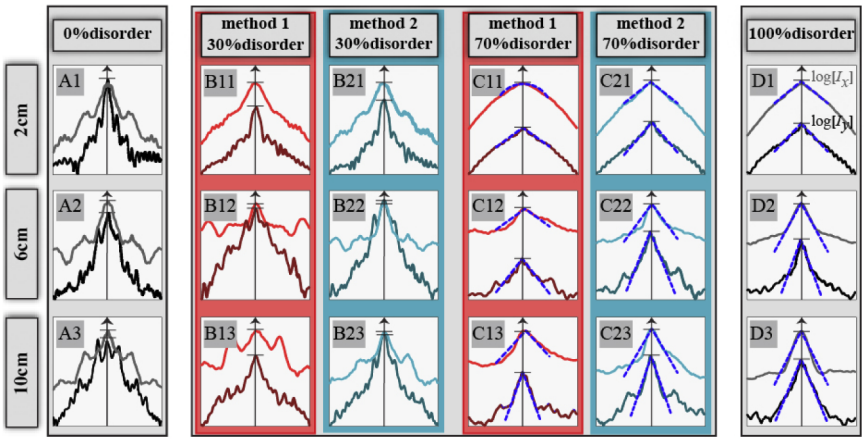

Fig. 6. Comparison of light localization along different directions. Log-plot cross sections of averaged intensity distributions along the x-axis (gray/red/cyan plots) and y-axis (black/dark red/ dark cyan plots), for different disorder strengths: (A) 0% , (B1), (B2) 30%, (C1), (C2) 70% and (D) 100%; blue dashed lines are corresponding linear fits. The horizontal axes span 400 μm in the x- and the y-direction. For each plot, there are two stacked vertical axes, where short horizontal bars are set on 1's. Other parameters are as in Fig. 2.

For 100% disorder, we notice even more pronounced localization with a longer propagation distance (Fig. 5 (D), and Fig. 6 (D)). Also, more pronounced localization is along the y-axis than the x-axis. Since, for 100% disorder, the original lattice does not contribute to anisotropy and the disorder pattern, we use in our study, does not have clear x-y anisotropy preference, we conclude

Optics EXPRESS

that the direction of crystal anisotropy is primarily cause of more pronounced localization in the y-direction. On the other hand, the asymmetry of log plots (along any axis and arbitrary disorder level) is due to the specific occurrence of the used disorder pattern. The influence of the disorder pattern anisotropy (not along x-y-direction) is noticeable at some probe beam transverse intensity distributions, as can be discerned comparing Figs. 5 (D2) - (D3) with Fig. 1 (B1).

To mitigate asymmetry of the log-plot cross-sections of averaged intensity distributions we use the average of the left and right sides of such profiles along the x-axis from the center. We fit such averaged log-plots cross sections and calculate the localization length according to Eq. (5) for disorder levels where the log-plot cross sections are linearly fitted. Figure 7 depicts a comparison of localization along the x-axis in our two methods for various disorder strengths and two propagation distances (4 cm and 8 cm). For lower disorder strengths we do not fit the log-plots (Figs. 7 (A1) and (B1)), where significant features of aperiodic lattices are remaining. However, we notice the spreading of the log-plots simultaneous with increased $\langle\omega_{\text{eff}}\rangle$, indicating that DET occurs. For both methods, at disorder strength between 50-60% at the shorter propagation distance (4 cm) light diffraction is closest to diffusive-like transport where the parabolic fits of the log-plots near the center could be attempted with low confidence (goodness of fit lower than 0.85). But, this tendency is further weakened at a longer propagation distance, so after 8 cm of propagation for 60% disorder log-plots are linearly fitted near the center indicating light localization (Fig. 7 (B2)). For higher disorder strength (80% and 100%) light localization is visible for the shorter propagation distance (4 cm, Fig. 7 (A2)), but more pronounced localization is evident for longer propagation distances also proved by linear fits of log-plots. One can see more pronounced localization for M2 than M1: log-plot fits for the same disorder level are steeper for M2, the slopes of the fits determine localization lengths.

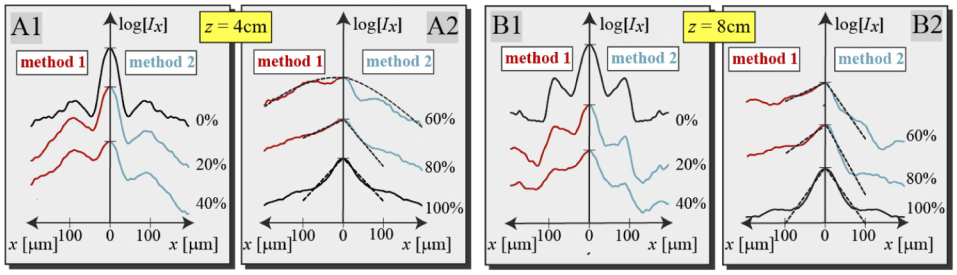

Fig. 7. Comparison of light localization in two methods for various disorder strengths and two propagation distances. Log-plot cross sections of intensity distributions symmetrized over left and right side of the x-direction, for M1 (left), M2 (right), and different disorder strengths after (A1)-(A2) 4 cm, and (B1)-(B2) 8 cm of propagation. The y-axes stacked similarly as in Fig. 6 and the other parameters are as in Fig. 2.

We characterize light localization by comparing the localization length (Eq. (5)) of linearly fitted log-plots along the x- and y-direction (Fig. 8) after 10 cm of propagation. The localization lengths in either direction are greater for M1 than for M2 indicating more pronounced localization for M2, qualitatively connecting lattice intensity with AL strength. For both methods, more pronounced localization is visible along the y-axis where the localization lengths have lower values comparing to the x-axis, due to the crystal and lattice anisotropy. One can see that differences between localization lengths are larger for lower disorder strengths, while their values converge to each other as disorder strength increases, meeting at 100% disorder strength; a similar conclusion stands for $\langle\omega_{\text{eff}}\rangle$s (Fig. 2 (A)). We notice that AL occurs at different disorder levels along different directions. Along the y-axis, localization appears for lower disorder strengths than along the x-axis. Figure 8 illustrates diffusive-like transport along the x-axis and light localization along the y-axis for the same 50%-60% disorder region.

Optics EXPRESS

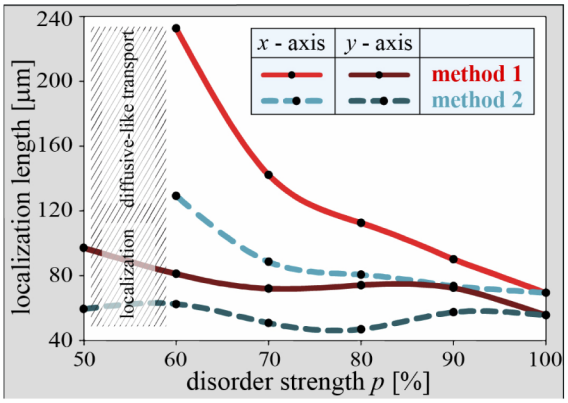

Fig. 8. Comparison of localization lengths after 10 cm of propagation distances for various disorder strengths for both methods and both the x- and y-directions. Other parameters are as in Fig. 2.

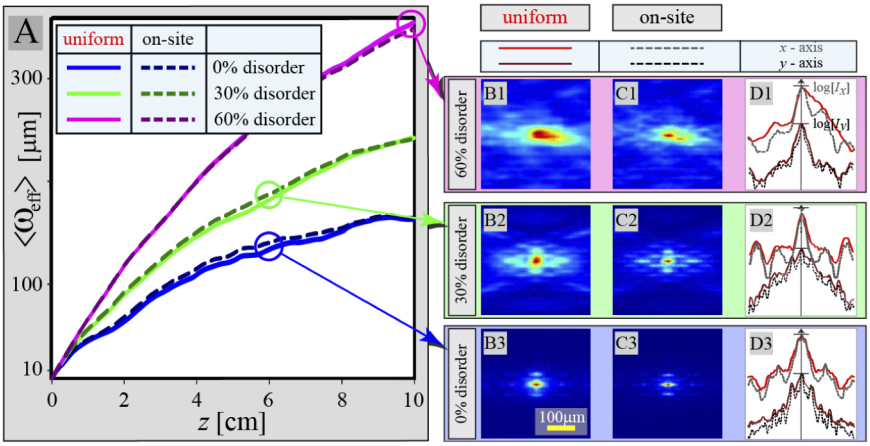

Fig. 9. Influence of probe beam excitation positions on the diffraction and localization (for M1). (A) $\langle\omega_{\text{eff}}\rangle$ versus propagation distances for uniform excitation positions and only on-site positions for different disorder strengths. (B) and (C) Appropriate averaged intensity distributions at the lattice output. (D) Log-plot cross sections of averaged intensity distributions along the x-axis (red/gray plots) and y-axis (dark red/black plots) for uniform and on-site positions for different disorder strengths. Other parameters are as in Fig. 2.

Optics EXPRESS

Moreover, we study the consequences of the choice of excitation probe beam positions distribution on the beam propagation. Statistics presented up to this point was based on the uniform distribution of probe beam excitations regardless of waveguide positions. Further, we investigate if the choice of only on-site excitation positions significantly changes the diffraction and localization characteristics. Figure 9 summarizes such results for M1. We compare $\langle\omega_{\text{eff}}\rangle$s for three disorder levels (Fig. 9 (A)) and observe slight differences between uniform and on-site excitation. Appropriate averaged intensity distributions are presented in Figs. 9 (B), (C) as well as their log-plots along the x- and y-axis (Fig. 9 (D)). We notice dissimilarity in $\langle\omega_{\text{eff}}\rangle$s for uniform one and on-site cases, at the different propagation distances for 0% and 30% disorder than for 60% disorder. $\langle\omega_{\text{eff}}\rangle$ has higher values for on-site excitation cases than for uniform, especially for lower disorder strengths (0% and 30%) after 6 cm propagation distance. However, for higher disorder strength (60%) $\langle\omega_{\text{eff}}\rangle$ is greater for uniform excitation case after 10 cm propagation distance. Such difference is caused by different computational spaces: the effective beam width is calculated for the whole computation space, with the significant contribution of tails in calculations, while the transverse intensity distributions and the log-plots are shown for the shorter (central domain), where tails contributions are discounted. Also, discrete diffraction is more pronounced for lower disorder strength for on-site excitation cases than for uniform cases, as is visible from intensity distributions and log-plots (Figs. 9 (B2) - (D2), and (B3) - (D3)). For 60% disorder, discrete diffraction is not observed for the on-site case, due to the diminished accuracy of on-site positions for higher disorder strengths. For all disorder strengths, the weaker difference is in log-plots along the y-direction. Asymmetry of log-plots is due to the specific occurrence of the used disorder pattern. However, the consequence of this choice is unsubstantial on statistical quantities.

In this research, we observe that dependence of light diffraction on various parameters is more noticeable for longer propagation. However, the question remains if the wider beams that are consequences of longer propagation distance lose their sensitivity to the local environment and thus hinder the accuracy of diffraction properties investigation. We observed different rates of increase of averaged effective beam width during propagation in our disordered lattices and consequently a variety of beam widths and shapes. Hence, we investigate the independent influence of probe beam width on light transport and localization in our disordered lattices in comparison to the free space propagation of the Gaussian beam. Figure 10 summarizes such results.

We choose three various input probe beam widths (8μm, 20μm, and 50μm). Averaged effective beam widths are considered along the propagation distance for different disorder strengths: 0%, 70%, and 100% (Fig. 10 (A)). More pronounced light transport is observed for narrower probe beam widths. Strong correlation of $\langle\omega_{\text{eff}}\rangle$ with I_{avg}^{-1} for input probe beam of 8μm presenting in Fig. 4, gradually diminish for wider probe beams. Also, wider probe beam reduces their sensitivity on disorder strength p and propagation distance, making wider beams less suitable for our investigation. Appropriate averaged intensity distributions after 4 cm propagation are presented in Figs. 10 (B), (C), (F). For 70% disorder, the log-plots along the different domains of the x-axis are shown in Fig. 10 (D) for different input probe beam widths, while Fig. 10 (E) present only their central domain along the x-axis of 400μm. We show that for all probe beam widths, along the x-axis in our disorder lattices light is spreading to the same degree as the Gaussian in free space propagation. Different domains along the x-axis represent the degree of diffraction for different probe beam widths (Fig. 10 (D)). However, a significant difference between the log-plots in our disordered lattice and the log-plots of Gaussian free space propagation is noticeable only in a limited central domain after the same propagation distance (Fig. 10 (E)). For narrow probe beam widths (8μm and 20μm), Figs. 10 (E1) (E2), localization occurs in the central domain with a size comparable to the size of the typical lattice pattern. In contrast, a wide probe beam (50μm)

Optics EXPRESS

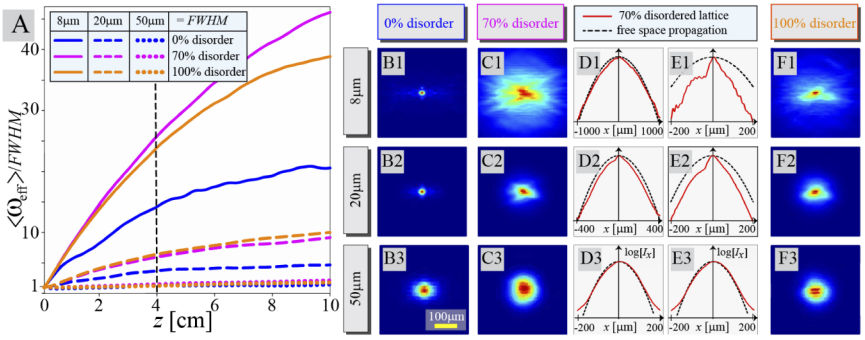

Fig. 10. Influence of probe beam width on the localization effects for M1. (A) Normalized $\langle\omega_{\text{eff}}\rangle$s versus propagation distances for three probe beam widths and different disorder strengths. Appropriate averaged intensity distributions after 4 cm (the dashed line in (A)) propagation distance for various disorder strengths: (B) 0%, (C) 70%, (F) 100%. (D) Log-plots of averaged intensity distributions along the x-axis in disordered lattice with 70% disorder strength compared with corresponding log-plots of Gaussian free space propagation. (E) The same log-plots along the x-axis as in (D) for narrow central domain from -200 to 200 μm. Other parameters are as in Fig. 2.

barely diffracts, i.e. propagates almost the same as a wide Gaussian beam in free space, limiting suitable widths of the probe beam for lattice excitation.

6. Conclusion

In this article, we presented two different theoretical methods for the realization of disordered two-dimensional photonic lattices optically induced in a photorefractive media. We numerically model light propagation in disordered aperiodic Mathieu lattices. We observed enhanced light transport for all disorder strengths but AL of light for higher disorder strengths in both methods. Localization effects are more pronounced for longer propagation distances. More pronounced localization is observed for M2 than M1: we attributed the difference between the two methods to various levels of lattice intensity. When studying the dependence of AL and DET on disorder level, to mitigate the influence of lattice intensity, we suggest further modification of our M2 in which averaged intensity levels are equalized for every disorder strength used. Localization length differs along different directions, due to the crystal and lattice anisotropy. There is no noticeable difference in localization effects if we choose only on-site probe beam excitation positions, as compared to uniform position distribution. For broad probe Gaussian beams localization is not observed in such lattices.

Funding. Ministry of Education, Science, and Technological Development of the Republic of Serbia .

Acknowledgments. The authors acknowledge funding provided by the Institute of Physics Belgrade and Institute for Multidisciplinary Research, through the grants by the Ministry of Education, Science, and Technological Development of the Republic of Serbia.

Disclosures. The authors declare no conflicts of interest.

Data availability. Data underlying the results presented in this paper are not publicly available at this time but may be obtained from the authors upon reasonable request.

References

1. P. W. Anderson, "Absence of diffusion in certain random lattices," Phys. Rev. **109**(5), 1492–1505 (1958).
2. H. De Raedt, A. Lagendijk, and P. de Vries, "Transverse localization of light," Phys. Rev. Lett. **62**(1), 47–50 (1989).
3. P. Sheng, *Scattering and Localization of Classical Waves in Random Media* (World Scientific, 1990), 2nd ed.

Optics EXPRESS

4. A. Lagendijk, B. Tiggelen, and D. S. Wiersma, "Fifty years of anderson localization," Phys. Today **62**(8), 24–29 (2009).
5. S. S. Abdullaev and F. K. Abdullaev, "On the light propagation in the system of tunnel-coupled waveguides," Sov. J. Radiofizika **23**, 766–767 (1980).
6. T. Pertsch, U. Peschel, J. Kobelke, K. Schuster, H. Bartelt, S. Nolte, A. Tünnermann, and F. Lederer, "Nonlinearity and disorder in fiber arrays," Phys. Rev. Lett. **93**(5), 053901 (2004).
7. Y. Lahini, A. Avidan, F. Pozzi, M. Sorel, R. Morandotti, D. N. Christodoulides, and Y. Silberberg, "Anderson localization and nonlinearity in one-dimensional disordered photonic lattices," Phys. Rev. Lett. **100**(1), 013906 (2008).
8. T. Schwartz, G. Bartal, S. Fishman, and M. Segev, "Transport and anderson localization in disordered two-dimensional photonic lattices," Nature **446**(7131), 52–55 (2007).
9. G. Kopidakis, S. Komineas, S. Flach, and S. Aubry, "Absence of wave packet diffusion in disordered nonlinear systems," Phys. Rev. Lett. **100**(8), 084103 (2008).
10. A. Szameit, Y. V. Kartashov, P. Zeil, F. Dreisow, M. Heinrich, R. Keil, S. Nolte, A. Tünnermann, V. Vysloukh, and L. Torner, "Wave localization at the boundary of disordered photonic lattices," Opt. Lett. **35**(8), 1172–1174 (2010).
11. L. Martin, G. D. Giuseppe, A. Perez-Leija, R. Keil, F. Dreisow, M. Heinrich, S. Nolte, A. Szameit, A. F. Abouraddy, D. N. Christodoulides, and B. E. A. Saleh, "Anderson localization in optical waveguide arrays with off-diagonal coupling disorder," Opt. Express **19**(14), 13636–13646 (2011).
12. U. Naether, Y. V. Kartashov, V. A. Vysloukh, S. Nolte, A. Tünnermann, L. Torner, and A. Szameit, "Observation of the gradual transition from one-dimensional to two-dimensional anderson localization," Opt. Lett. **37**(4), 593–595 (2012).
13. S. Stützer, Y. V. Kartashov, V. A. Vysloukh, A. Tünnermann, S. Nolte, M. Lewenstein, L. Torner, and A. Szameit, "Anderson cross-localization," Opt. Lett. **37**(10), 1715–1717 (2012).
14. M. Boguslawski, S. Brake, J. Armijo, F. Diebel, P. Rose, and C. Denz, "Analysis of transverse anderson localization in refractive index structures with customized random potential," Opt. Express **21**(26), 31713–31724 (2013).
15. D. M. Jović and M. R. Belić, "Steady-state and dynamical anderson localization of counterpropagating beams in two-dimensional photonic lattices," Phys. Rev. A **81**(2), 023813 (2010).
16. D. M. Jović, Y. S. Kivshar, C. Denz, and M. R. Belić, "Anderson localization of light near boundaries of disordered photonic lattices," Phys. Rev. A **83**(3), 033813 (2011).
17. D. M. Jović, M. R. Belić, and C. Denz, "Transverse localization of light in nonlinear photonic lattices with dimensionality crossover," Phys. Rev. A **84**(4), 043811 (2011).
18. C. Conti and A. Fratalocchi, "Dynamic light diffusion, three-dimensional anderson localization and lasing in inverted opals," Nat. Phys. **4**(10), 794–798 (2008).
19. Z. Vardeny, A. Nahata, and A. Agrawal, "Optics of photonic quasicrystals," Nat. Photonics **7**(3), 177–187 (2013).
20. L. Negro and S. Boriskina, "Deterministic aperiodic nanostructures for photonics and plasmonics applications," Laser Photonics Rev. **6**(2), 178–218 (2012).
21. E. Maciá, "The role of aperiodic order in science and technology," Rep. Prog. Phys. **69**(2), 397–441 (2006).
22. J. V. Vasiljević, A. Zannotti, D. V. Timotijević, C. Denz, and D. M. J. Savić, "Creating aperiodic photonic structures by synthesized mathieu-gauss beams," Phys. Rev. A **96**(2), 023840 (2017).
23. A. Zannotti, J. M. Vasiljević, D. V. Timotijević, D. M. J. Savić, and C. Denz, "Morphing discrete diffraction in nonlinear mathieu lattices," Opt. Lett. **44**(7), 1592–1595 (2019).
24. M. V. Berry and N. L. Balazs, "Nonspreading wave packets," Am. J. Phys. **47**(3), 264–267 (1979).
25. E. G. Kalnins and J. W. Miller, "Lie theory and separation of variables. 9. orthogonal r-separable coordinate systems for the wave equation $\psi_{tt} - \triangle_2\psi = 0$," J. Math. Phys. **17**(3), 331–355 (1976).
26. J. Durnin, J. J. Miceli, and J. H. Eberly, "Diffraction-free beams," Phys. Rev. Lett. **58**(15), 1499–1501 (1987).
27. J. C. Gutiérrez-Vega, M. D. Iturbe-Castillo, and S. Chávez-Cerda, "Alternative formulation for invariant optical fields: Mathieu beams," Opt. Lett. **25**(20), 1493–1495 (2000).
28. M. A. Bandres, J. C. Gutiérrez-Vega, and S. Chávez-Cerda, "Parabolic nondiffracting optical wave fields," Opt. Lett. **29**(1), 44–46 (2004).
29. B. Freedman, G. Bartal, M. Segev, R. Lifshitz, D. N. Christodoulides, and J. Fleisher, "Wave and defect dynamics in nonlinear photonic quasicrystals," Nature **440**(7088), 1166–1169 (2006).
30. M. Boguslawski, N. M. Lučić, F. Diebel, D. V. Timotijević, C. Denz, and D. M. J. Savić, "Light localization in optically induced deterministic aperiodic fibonacci lattices," Optica **3**(7), 711–716 (2016).
31. J. M. Vasiljević, A. Zannotti, D. V. Timotijević, C. Denz, and D. M. J. Savić, "Light propagation in aperiodic photonic lattices created by synthesized mathieu–gauss beams," Appl. Phys. Lett. **117**(4), 041102 (2020).
32. L. Levi, M. Rechtsman, B. Freedman, T. Schwartz, O. Manela, and M. Segev, "Disorder-enhanced transport in photonic quasicrystals," Science **332**(6037), 1541–1544 (2011).
33. S. Longhi, "Inverse anderson transition in photonic cages," Opt. Lett. **46**(12), 2872–2875 (2021).
34. A. Zozulya and D. Anderson, "Propagation of an optical beam in a photorefractive medium in the presence of a photogalvanic nonlinearity or an externally applied electric field," Phys. Rev. A **51**(2), 1520–1531 (1995).
35. G. Agrawal, *Nonlinear Fiber Optics* (Academic Press, 2012), 5th ed.
36. Z. Bouchal, "Nondiffracting optical beams: Physical properties, experiments, and applications," Czech. J. Phys **53**(7), 537–578 (2003).